IOP Publishing Journal of Physics: Condensed Matter
J. Phys.: Condens. Matter **32** (2020) 135503 (8pp) https://doi.org/10.1088/1361-648X/ab5f37

# Boron-dopant enhanced stability of diamane with tunable band gap

**Caoping Niu[1,2], Ya Cheng[1,2], Kaishuai Yang[1,2], Jie Zhang[1], Hanxing Zhang[1,2], Zhi Zeng[1,2] and Xianlong Wang[1,2,3]**

[1] Key Laboratory of Materials Physics, Institute of Solid State Physics, Chinese Academy of Sciences, Hefei 230031, People's Republic of China
[2] University of Science and Technology of China, Hefei 230026, People's Republic of China

E-mail: xlwang@theory.issp.ac.cn

Received 27 September 2019, revised 22 November 2019
Accepted for publication 5 December 2019
Published 2 January 2020

**Abstract**

The structural, electronic, and superconducting properties of B-doped cubic and hexagonal diamane (single layer diamond) were investigated based on the first-principles methods. B atom tends to stay in the substitutional site, and the most stable configuration is the structure with vertical B–B dimer. The formation energy of B-doped diamane is lower than the counterpart of pristine diamane indicating that B dopant can facilitate the synthesis of diamane. The configurations with vertical B–B dimers are semiconductors with tunable band gaps, which decrease with the B concentration increasing due to the interaction between B–B dimers. For example, the band gap of 3.125 mol% and 6.25 mol% B-doped cubic diamane is 1.82 eV and 1.44 eV, respectively. Moreover, configurations with meta-stable B distributions are metals, which have comparable superconducting transition temperatures with B-doped diamond (~4 K).

Keywords: first-principles, diamane, boron dopant, tunable gap, superconductivity

(Some figures may appear in colour only in the online journal)

## 1. Introduction

Since graphene was synthesized by micromechanical stripping in 2004 [1], two-dimensional (2D) materials have attracted wide attention. To date, many kinds of 2D materials have been synthesized, such as hexagonal boron nitride, molybdenum disulfide, and transition metal chalcogenides [2–4], which have broad applications in energy storage, catalysis, and electronics [5–9]. Therefore, it is important to explore new 2D materials and extend their applications. Graphene and diamond are the allotropes of carbon with 2D and three-dimensional (3D) structure, respectively, and both of them have unique physical and chemical properties. Formation of $sp^3$ bonds between bi-layer graphene can give rise to a single-layer diamond, named as diamane, which has the characteristics of both graphene and diamond. For example, theoretical predictions shown that the band gap of diamane is about half of the diamond [10–12], and the Young's modulus of diamane is higher than graphene and graphane [12–14]. Diamane is expected to be a new carbon based 2D material with excellent properties. Both theoretical [15–24] and experimental [13, 25–27] works have focused extensively on the synthesis mechanism and properties of diamane.

Because graphite can be converted into diamond under high-temperature and high-pressure [28–30], experimental works tried to synthesize the diamane via the pressurization of bi-layer graphene [13, 25, 27]. Simulations based on the first-principles methods shown that diamane can exist at ambient conditions [15–18], which indicates that the diamane synthesized at high-pressure condition can be stored under ambient pressure. Bi-layer graphene were compressed by using diamond anvil cell (DAC), and the measurements of hardness, refractive index, and Raman spectroscopy of the samples show that the samples had the characteristics of $sp^3$ bond under high-pressure [25]. However, $sp^3$ signals disappeared after releasing the pressure. In addition, diamane was synthesized

[3] Author to whom all correspondence should be addressed.

 

based on the atomic force microscopy (AFM) by extrusion of bi-layer graphene, while it returned to bi-layer graphene after the extrusion was removed [13]. So far, researchers could not get the high-pressure synthesized diamane at the ambient conditions. It is necessary to find an effective way to enhance the stability of diamane and extend its applications.

Since the radius of the B atom is comparable to that of the C atom, B-dopant is an efficient way to extend the applications of carbon systems [31–36]. For example, B-dopant can open the band gap and enhance the lithium storage of graphene [31–33], and B-dopant can cause insulator–metal transition in diamond [35, 36]. This inspired us to investigate the effect of B-dopant on the stability and physical properties of diamane. We found that B atoms in the diamane tend to gather together and can tune the band gap. The superconducting transition temperatures of metallic B-doped diamane are also explored. Furthermore, our results show that B-dopant can reduce the formation energy (FE) of diamane from bi-layer graphene. Interestingly, since the diamane with F saturation is more stable than that of H saturation [12], a large area of fluorinated diamane was recently synthesized at ambient conditions based on the chemical vapor deposition (CVD) method [37], which indicates that B dopant may also be used to promote the synthesis of diamane.

## 2. Methods

The calculation of structural and electronic properties were carried out based on the density functional theory as implemented in the Vienna *ab initio* approximation package (VASP) [38, 39]. The generalized gradient approximation (GGA) [40] functional parametrized by the Perdew–Burke–Ernzerhof (PBE) [41] and projector-augmented plane-wave (PAW) potentials were used for calculations. The structures were fully relaxed with a cutoff energy of 400 eV, and the convergence of energy and force were set to $1 \times 10^{-6}$ eV and 0.001 eV Å$^{-1}$, respectively. Two types of diamane, cubic diamane (CD) and hexagonal diamane (HD), were investigated, and the structures are shown in figure 1. For investigation of the B atom distribution, the supercells constructed by $2 \times 2$ and $4 \times 2$ primitive cells with B concentration of 6.25 mol% were used. The effects of B concentrations on the band gap of diamane were studied by using the $n \times m$ $(3 \leqslant n \leqslant 7, 1 \leqslant m \leqslant 6)$ supercells with the concentrations ranging from 1.19 mol% to 16.67 mol%, where $n(m)$ means the number of primitive unit cells along $x(y)$ direction (as shown in figure 1). The vacuum layer was set to 20 Å, which is enough to avoid the interaction between the neighboring diamane layers. Reciprocal space was represented by using the Monkhorst–Pack scheme [42], and the number of $k$-points ensure the convergence of energies within 0.5 meV/atom. The phonon dispersions were calculated by using the PHONOPY code. All structures used for calculating the FE of diamane were optimized by using the *optPBE-vdW* method [43, 44], which included van der Waals force correction between bi-layer graphene.

The electron–phonon coupling (EPC) parameter $\lambda$ was carried out by using the density-functional perturbation theory (DFPT) [45] as implemented in the QUANTUM ESPRESSQ [46] based on Bardeen–Cooper–Schrieffer (BCS) theory [47], with Norm–Conserving pseudopotentials. All structures were optimized until the forces on each atom reached $10^{-2}$ Ry/au. The self-consistency criteria for total energies was set at $10^{-8}$ Ry, with a plane-wave energy cutoff set 60 Ry. We used $4 \times 4 \times 1$ $q$-point meshes for EPC parameter $\lambda$.

## 3. Results and discussion

### 3.1. Boron distribution features

Similar to the existing theoretical results about pristine diamane [14, 21], our results show that CD is more stable than HD with the energy difference of 2.816 meV/atom. In addition, we also calculated the thermodynamic properties of pristine diamane based on the quasi-harmonic approximation (QHA), and the Helmholtz free energy of CD is 4.285 meV/atom and 8.706 meV/atom lower than that of HD at the temperature of 300 K and 1000 K, respectively. This suggests that the stability of CD will increase with temperature increasing. The Interlayer C–C bond length of CD and HD are 1.56 Å and 1.59 Å, respectively, which is the same as previous reported values (1.56 Å and 1.59 Å) [21]. Furthermore, the simulated bandgap with GGA–PBE method of the CD (3.04 eV) is larger than that of HD (2.86 eV) agreeing with the previous report [14]. Since the PBE functional underestimates the band gap, we calculated the band gap again using the hybridized functional (HSE06). We find that the band gap of CD and HD is 4.20 eV and 4.05 eV, respectively, which is about 1.2 eV larger than the values calculated based on the PBE functional. However, the band gap difference between CD and HD does not change much, which indicate that PBE functional can sufficiently describe the band gap discrepancies of diamane in different phases. These results show that our used methods and parameters can describe the properties of diamane well.

We first investigated stable configurations of B-doped diamane in a $2 \times 2$ supercell (16 C atoms) with one B dopant corresponding to the concentration of 6.25 mol%. There are two substitutional sites (site-1 and site-2) and one interstitial site (site-3), as shown in figure 1. We studied the stability of H saturation when B atom located at the substitutional site-2, and the results show that it tends to be H terminated. Therefore, in the following study, we only considered the H terminated configuration when B substitute at the site-2. For both CD and HD, the total energy of B located at the substitutional site-1 is 0.02 eV and 0.11 eV lower than that at the substitutional site-2, respectively. Furthermore, we calculated the energy differences between the cases of B at the substitutional site-1 and at the interstitial site-3 by using the following formula:

$$\Delta E = E_{\text{sub}} - E_{\text{inter}} + E_{\text{sp}^3\text{–}C} \tag{1}$$

where $E_{\text{sub}}$ ($E_{\text{inter}}$) represent the total energy of B at the substitutional site-1 (interstitial site-3), and $E_{\text{sp}^3\text{–}C}$ is taken as the energy of one sp$^3$-type C atom in the diamond (−9.09 eV). For all investigated configurations, negative $\Delta E$ values are obtained. For example, $\Delta E$ is −3.68 eV in 6.25 mol% B doped CD. The result indicates that B atom tend to stay at the

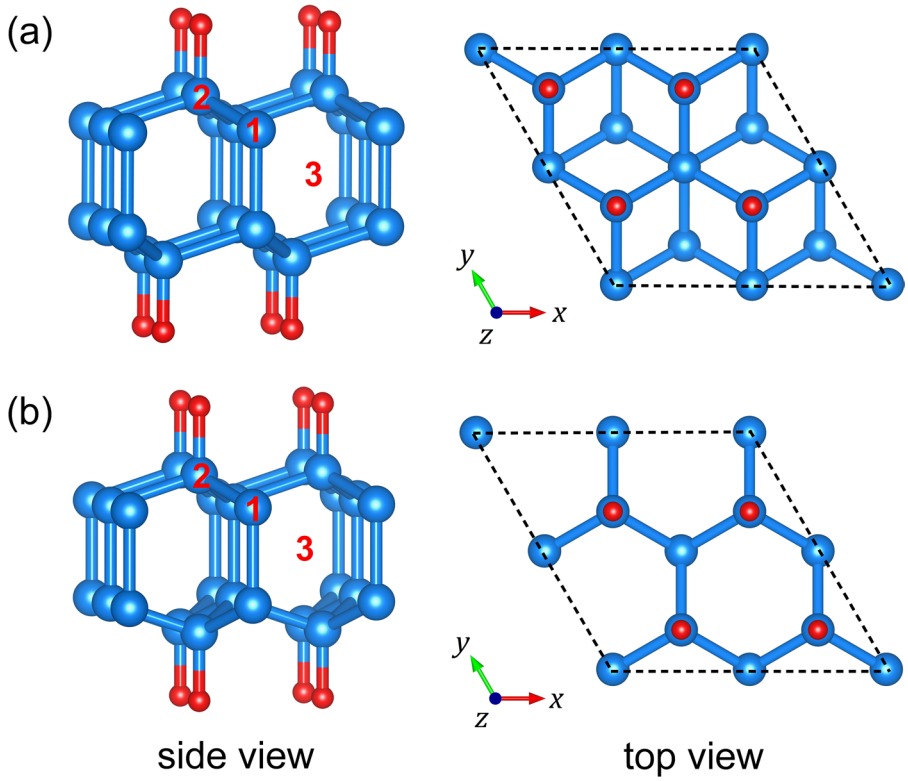


**Figure 1.** Configurations of cubic diamane and hexagonal diamane are shown in (a) and (b), respectively. Left (right) part is the side (top) view. C and H atoms are shown in blue and red, respectively. For B dopant, there are three non-equivalent positions, substitutional site-1, substitutional site-2, and interstitial site-3, which are marked by the red numbers in the side view.

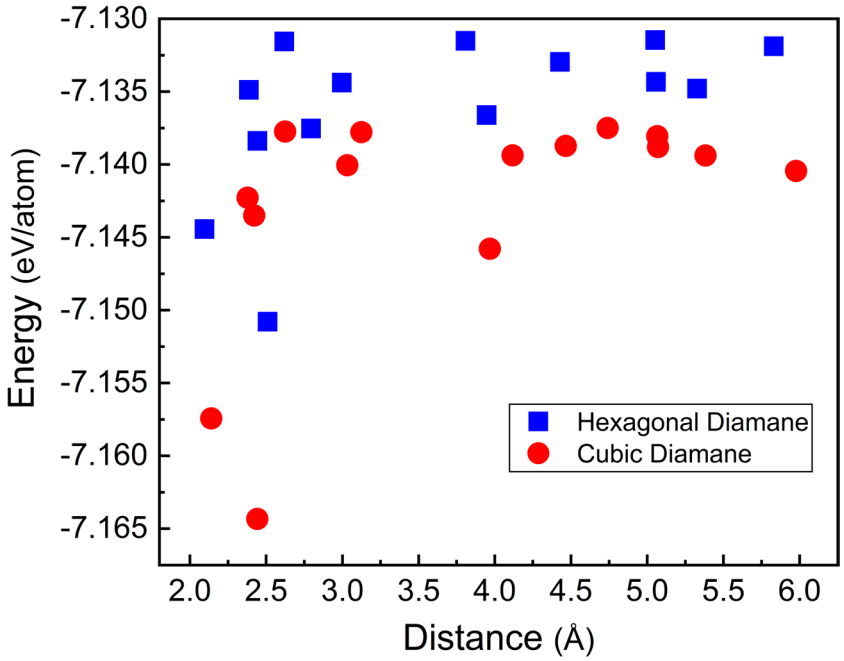


**Figure 2.** Energies of the 4 × 2 supercells with two substituted B atoms (6.25 mol% B dopant) are shown as a function of B–B distance.

substitutional sites but not interstitial site. Following, we will focus on the cases of B at the substitutional sites. In the next paragraph, we will discuss the interaction between two substituted B atoms in the larger supercell with 32 C atoms (6.25 mol% B dopant) constructed by 4 × 2 primitive cell.

There are 29 non-equivalent configurations for two substituted B atoms in the 4 × 2 supercell, and the total energies of all non-equivalent configurations are shown in the figure 2 as a function of B–B distance. It can be seen that similar to the pristine diamane, B-doped CD have lower energies than

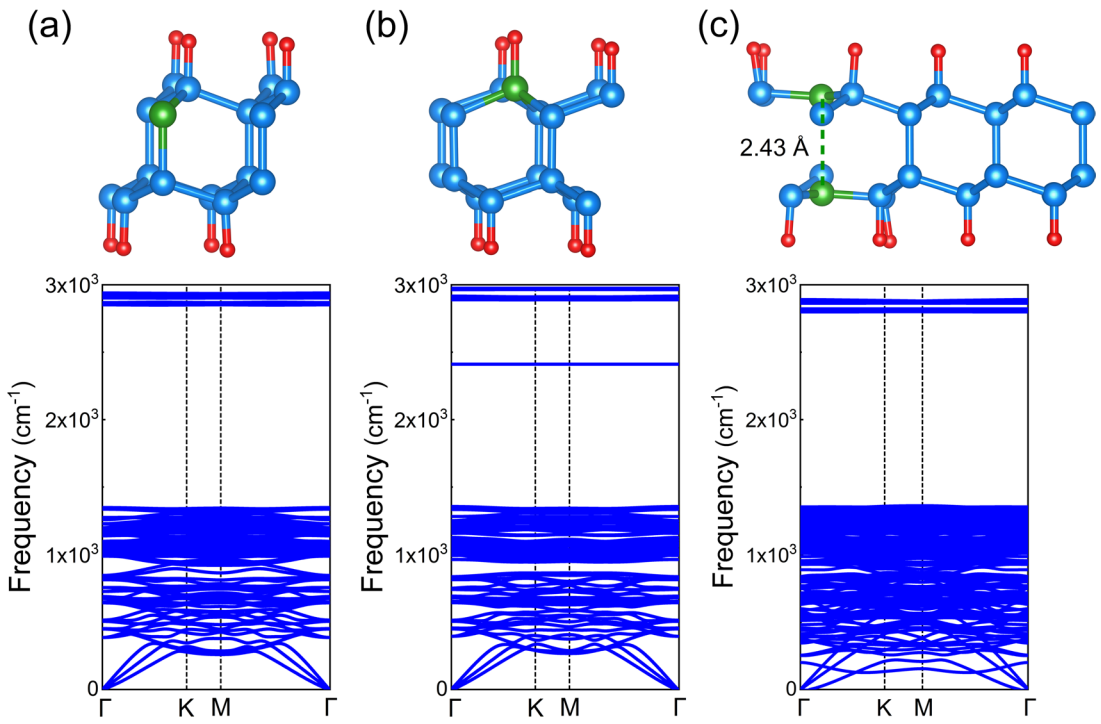


**Figure 3.** The up-part shows the configurations of one B atom at the substitutional site-1 (a), substitutional site-2 (b), and two B atoms form vertical B–B dimer (c) in cubic diamane, corresponding to the concentration of 6.25 mol%. For each configuration, the phonon dispersions are shown in the down-part. C, B, and H atoms are shown in blue, green, and red, respectively. The dashed green line shows the distance (2.43 Å) between two B atoms in the vertical B–B dimer.

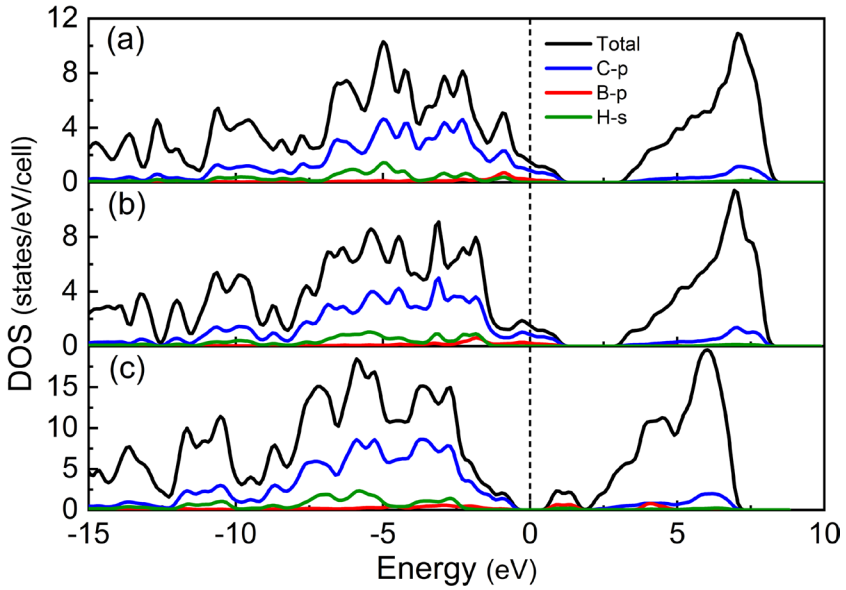


**Figure 4.** Total and partial density of states of 6.25 mol% B doped cubic diamane (CD), with one B atom at the substitutional site-1 (a), substitutional site-2 (b), and vertical B–B dimer (c). The Fermi level is set to zero.

the B-doped HD. Moreover, in the range of short B–B distance (<3.2 Å), the energy increases with the B–B distance increasing, and it reach a plateau after the B–B distance longer than 3.2 Å, where B–B interactions vanish. The results show that different from B-doped graphene [48], B atoms tend to gather together. For both CD and HD, the most stable configuration is that two B atoms form vertical B–B dimer, and corresponding structure of CD is shown in figure 3(c). In this configuration, the B atom and three neighboring C atoms locate at the same plane with a B–C bonds of 1.55 Å, and the local environment of B atom is similar to $BH_3$, which indicate that the three valence electrons of B atom are saturated. The B–B distance in the vertical B dimer is 2.43 Å resulting in a very weak B–B interaction, and the same phenomenon is also observed in HD. This is different from the B–B dimer in diamond [49], where the B atoms deviate (~0.4 Å) from the

**Table 1.** Formation energy (FE) of pristine, 3.125 mol%, and 6.25 mol% B-doped diamane.

| | | 3.125 mol% B-doped diamane | | | 6.25 mol% B-doped diamane | | |
|---|---|---|---|---|---|---|---|
| FE (meV/atom) | Pristine diamane | Site-1 | Site-2 | Vertical B–B dimer | Site-1 | Site-2 | Vertical B–B dimer |
| CD | −27.1 | −20.6 | −20.1 | −32.7 | −21.1 | −21.7 | −41.5 |
| HD | −19.9 | −15.1 | −13.6 | −22.4 | −17.4 | −15.8 | −27.7 |

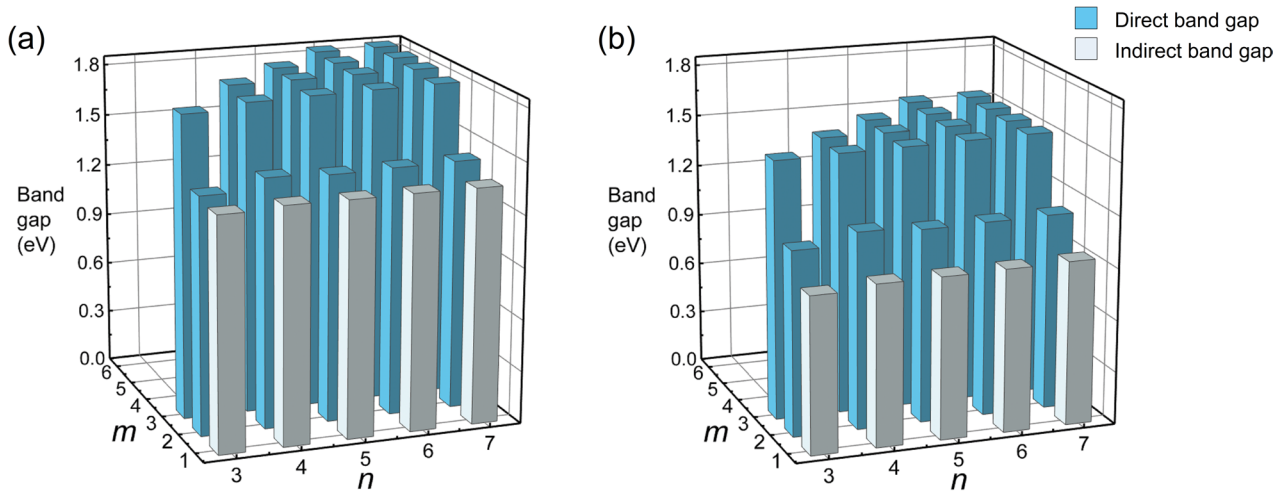


**Figure 5.** The calculated band gaps of cubic (a) and hexagonal (b) diamane by using the $n \times m$ supercells with one vertical B–B dimer, where $n$ and $m$ means the number of primitive unit cells along $x$ and $y$ direction, respectively. The semiconductors with direct and indirect band gap are shown in blue and grey colors, respectively.

plane formed by their three neighboring C atoms with a B–B distance of 1.95 Å. Since the diamane does not have the 3D $sp^3$ carbon network as in the diamond, the B–B vertical dimer in diamane can relax its structure sufficiently giving rise to a longer B–B dimer distance than that in diamond. In addition, we studied the interaction between two B–B dimers in the $7 \times 6$ diamane supercell, and the results indicated that B–B dimers tend to be discretely distributed.

The configurations of one B atom located at substitutional site-1 and substitutional site-2 are shown in figures 3(a) and (b), respectively. In both of them, B atom has four neighbor atoms, and $sp^3$ B–C bands can be observed. The bond length of $sp^3$ B–C band is 1.59 Å closed to the $sp^3$ C–C bands (1.54 Å), and the local distortion around B atom is small. Since B atom has three electrons, the most stable configuration should be the one with three neighbors forming a plane structure similar to $BH_3$. Therefore, the vertical B–B dimer with $BH_3$-type local configure is more stable than others with $sp^3$ B–C bonds. The calculated phonon dispersions are also shown in figure 3, and the absence of virtual frequency indicates that diamanes with one B atom at the substitutional site or with vertical B–B dimer are dynamically stable.

In the following, we will present the FE of B-doped diamane. Usually, the FE is calculated with respect to the most stable form of its elements. But in this work, we are more inclined to the clarify formation energies of diamane from bi-layer graphene, which are generally used in experiments. Therefore, we defined the FE of diamane with H termination from bi-layer graphene based on the following formula:

$$\Delta E = \left(E_{\mathrm{dia}} - E_{\mathrm{gra}} - \frac{n}{2}E_{\mathrm{H_2}}\right)/3n \tag{2}$$

where $E_{\mathrm{dia}}$ ($E_{\mathrm{gra}}$) represent the energy of diamane (bi-layer graphene) with or without B dopant. $E_{\mathrm{H_2}}$ is the energy of hydrogen molecules (−6.83 eV), and $n$ is the number of H atom ($3n$ is the number of atoms of diamane, because the number of C atoms is twice that of H atoms.). For 6.25 mol% (3.125 mol%) B-doped cases, $2 \times 2$ ($4 \times 2$) and $4 \times 2$ ($4 \times 4$) supercells are used for the configurations with one B atom substitution and vertical B–B dimer, respectively. The calculated results were shown in table 1, the FE of pristine CD and HD is −27.1 meV/atom and −19.9 meV/atom, respectively, which is consistent with the previous published results [21, 23]. We can find that one B atom substitution and vertical B–B dimer can increase and decrease the FE, respectively. For example, in the case of 6.25 mol% B-doped CD, the FE with one B atom substitution and vertical B–B dimer is −21.7 meV/atom and −41.5 meV/atom, respectively. Furthermore, the FEs of 3.125 mol% B-doped case are smaller than that of diamane with 6.25 mol% B-dopant, and increase of B concentration can decrease the FE. The result indicate that B dopant can promote the synthesis of diamane.

### 3.2. Electronic structures

Our calculated electronic structures show that B-doped diamane with vertical B–B dimer is a semiconductor, however, others are metals. As an example, the density of states (DOS)

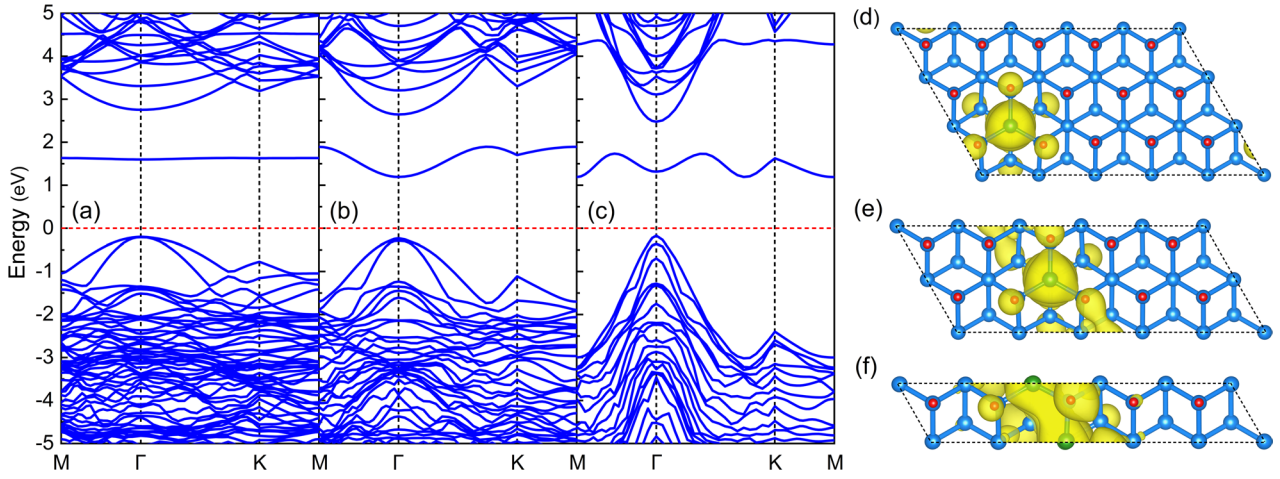


**Figure 6.** The band structures of vertical B–B dimer in 5 × 3 (a), 5 × 2 (b), and 5 × 1 (c) supercells of cubic diamane, corresponding to the concentration of 3.33 mol%, 5 mol% and 10 mol%, respectively. The red dotted line indicates the Fermi level. (d), (e) and (f) show the partial charge density of impurity band in 5 × 3, 5 × 2, and 5 × 1 supercells with an isosurface level of 0.003 $a_0^{-3}$ ($a_0$: Bohr radius).

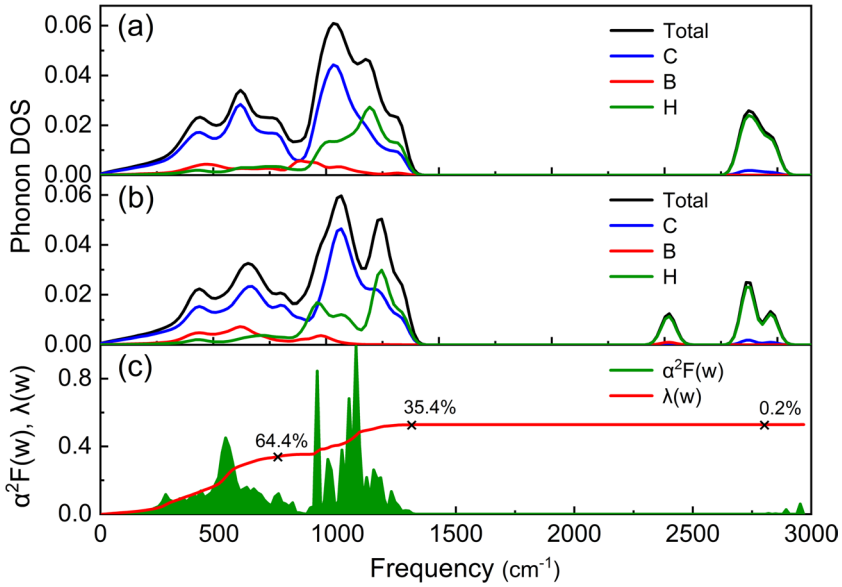


**Figure 7.** Partial phonon density of states of 12.5 mol% B doped cubic diamane with one B atom at the substitutional site-1 (a) and substitutional site-2 (b). (c) shows the Eliashberg phonon spectral function $\alpha^2F(w)$ and EPC parameter $\lambda$ of 12.5 mol% B doped cubic diamane with one B atom at the substitutional site-1.

of 6.25 mol% B-doped CD with one B atom in the substitutional site-1 and site-2 are shown in figures 4(a) and (b), respectively. It can be seen that B atom hybridized strongly with the neighboring C atoms, and the electronic state at the Fermi level is mainly contributed by the *p*-orbitals of B atom and C atom. In these cases, B atom formed four covalent bonds with neighbors giving rise to hole dopant in the carbon network. As shown in figure 4(c), a band gap of 1.44 eV is observed in the 6.25 mol% B-doped CD with the vertical B–B dimer, where the interaction between two B atoms is very weak and three B electrons contribute to the three B–C covalent bonds without hole dopant.

In this paragraph, we will discuss the effects of the dimer concentrations on the band gap of diamane based on 25 different supercells ($n \times m, 3 \leqslant n \leqslant 7, 1 \leqslant m \leqslant 6$) with one vertical B–B dimer corresponding to the B concentrations of 1.19 mol% ~16.67 mol%. The calculated band gaps of CD and HD by using GGA functional are shown in figure 5 as functions of $n$ and $m$. Generally, the band gap decreases with the concentration of the vertical B–B dimer increasing. For the case of CD, the band gap gradually decreases from 1.84 eV to 1.74 eV, when the distance between two dimers changes from $m = 6$ to $m = 3$. The band suddenly decrease to 1.36–1.44 eV in the cases of $m = 2$. Detailed analysis shows that the systems with $m > 2$ are semiconductors with a direct band gap, and both the top of valence band and the bottom of conduction band locate at Γ point. Moreover, narrow indirect band gaps (1.34–1.36 eV) are observed when $m = 1$ with the bottom of

conduction band at M point. If the systems with the same $n$ values, their band gaps will increase with $m$ increasing due to the weaker interaction between B–B dimers along $y$ direction.

To clearly explain the physical reason for the evolution behaviors mentioned above, the band structures of vertical B–B dimer in $5 \times 3$, $5 \times 2$, and $5 \times 1$ supercells of CD are shown in the figure 6. We can find that the band gap is determined by the profile of the impurity band located in the band gap, which comes from the unoccupied B-$p$ orbitals. For the cases of $m > 3$, the impurity band is almost flat, since the interaction between B–B dimers is weak. However, dispersions are observed in the configurations of $m < 3$, and the dispersion of $m = 1$ is larger than that of $m = 2$. From the partial charge densities shown in figure 6, non-interaction, indirect-interaction via neighboring atoms, and direct-interactions between B–B dimers are observed in the cases of $m > 3$, $m = 2$, and $m = 1$, respectively, which caused the band gap discrepancies. Please note, above analysis also can be applied to B-doped HD, and the band gaps of B-doped HD are about 0.38 eV smaller than that of B-doped CD. Please note that, the GGA method underestimates the band gap. Nevertheless, our test calculations show that for different phases (CD or HD) and different B concentrations (6.25 mol% and 12.5 mol%), the calculated band gaps based on HSE06 are about 1.56 eV larger than that of GGA. Therefore, we believe that the band gap discrepancies of B-doped diamane calculated by GGA method is reliable, and the band gaps calculated by HSE06 can generally be obtained by adding 1.56 eV to the counterparts based on the GGA method.

In a word, B dopant can adjust the band gap of diamane and realize metallization, which are determined by B distribution features and B concentrations. Our results can give instructions to experiments for synthesizing the B-doped diamane with different properties. For example, a metallic B-doped diamane can be obtained by compressing one pristine graphene and one B-doped graphene, and a semiconductor may can be synthesized via the pressurization of bi-layer B-doped graphene.

### 3.3. Superconductivity

Finally, we present the superconducting properties of the metal phases with B concentrations of 12.5 mol%, and the phonon density of states are shown in figures 7(a) and (b). The total phonon density can be divided into three parts. The low frequency region of less than 750 $cm^{-1}$ is mainly derived from the stretching vibration of the C–C bond and the C–B bond. The intermediate frequency region (750–1400 $cm^{-1}$) mainly come from the shear vibration of C–H bond or B–H bond. And the high frequency region of more than 2400 $cm^{-1}$ is caused by the tensile vibration of the B–H bond and the C–H bond.

The Eliashberg phonon spectral function $\alpha^2F(w)$ and EPC parameter $\lambda$ for internal substitutional sites of 12.5 mol% B-doped CD were shown in figure 7(c), where $\lambda$ was defined as

$$\lambda(w) = 2\int_0^w \frac{\alpha^2F(w)}{w}\mathrm{d}w. \quad (3)$$

As seen from figure 7(c), $\lambda$ is small. The vibrations in the low frequency and intermediate frequency regions contribute 64.4% and 35.4%, respectively, while only 0.2% of the $\lambda$ parameter comes from the high frequency region. The main contributions to the electron–phonon coupling is the C–B bonds vibration. For different phases (CD or HD) and different B substitutional site (site-1 or site-2), a $T_c$ of ~4.0 K is found close to the $T_c$ of B-doped diamond [36, 50]. The results indicate that the $T_c$ of B-doped dimane is not sensitive to the B substitutional sites. However, the $T_c$ of B-doped diamane is much lower than that of B-doped graphane (45–77 K) [51, 52]. This is partially due to the fact that there are only one $sp^3$ hybridized C layer in the B-doped graphane, which may give larger electron–phonon coupling parameter ($\lambda = 0.72$) than that of B-doped diamane ($\lambda = 0.53$) with two $sp^3$ hybridized C layers. Furthermore, our further calculations show that $T_c$ of 6.25% B-doped CD with B atom at substitutional site-1 and substitutional site-2 are about 1.3 K, which is smaller than that of 12.5 mol% B-doped cases. Detailed electronic structure analyses show that the smaller $T_c$ in 6.25 mol% B-doped dimane may be caused by the lower density of states at the Fermi level. The results about B-doped graphane and B-doped diamane indicate that B-doped multilayer diamond films with more than one $sp^3$ hybridized C layer will have comparable $T_c$ with that of B-doped diamond.

## 4. Conclusions

Based on the first-principles methods, we studied the stability, electronic structures, and superconducting property of B-doped diamane. Both in cubic diamane and hexagonal diamane, B atoms tend to gather together. The cubic diamane with B dopant is more stable than B-doped hexagonal diamane. The B dopant can enhance the stability of diamane and can promote the diamane synthesis. Depending on the concentrations and distributions of B atoms, diamane with B dopants has variable electronic structures, metal or semiconductors with band gap ranging from 1.34 eV to 1.84 eV. The superconducting transition temperature of B-doped diamane is comparable to that of diamond with B dopant. Due to its adjustable band gap and 2D feature, B-doped diamane may can be used in electronic devices. Our work proposes a new scheme to stabilize the diamane with tunable function.

## Acknowledgments

This research was supported by the NSFC under Grant of 11674329, Science Challenge Project No. TZ2016001, and the Major/Innovative Program of Development Foundation of Hefei Center for Physical Science and Technology. The calculations were partly performed in Center for Computational Science of CASHIPS, the ScGrid of Supercomputing

Center and Computer Network Information Center of Chinese Academy of Sciences.

## ORCID iDs

Caoping Niu https://orcid.org/0000-0002-3330-7389
Ya Cheng https://orcid.org/0000-0003-3635-3652
Kaishuai Yang https://orcid.org/0000-0002-5170-728X
Xianlong Wang https://orcid.org/0000-0002-6514-9987

## References

[1] Novoselov K S, Geim A K, Morozov S V, Jiang D, Zhang Y, Dubonos S V, Grigorieva I V and Firsov A A 2004 *Science* **306** 666–9
[2] Watanabe K, Taniguchi T and Kanda H 2004 *Nat. Mater.* **3** 404–9
[3] Zhou W, Zou X, Najmaei S, Liu Z, Shi Y, Kong J and Lou J 2013 *Nano Lett.* **13** 2615–22
[4] Wang Q H, Kalantar-Zadeh K, Kis A, Coleman J N and Strano M S 2012 *Nat. Nanotechnol.* **13** 699–712
[5] Kim G, Kim M, Hyun C, Hong S, Ma K Y, Shin H S and Lim H 2016 *ACS Nano* **10** 11156–62
[6] Song D, Wang Y, Lu X, Gao Y, Li Y and Gao F 2018 *Sensors Actuators* B **267** 5–13
[7] Huang Y, Guo J, Kang Y, Ai Y and Li C M 2015 *Nanoscale* **7** 19358–76
[8] Chen W, Hou X, Shi X and Pan H 2018 *ACS Appl. Mater. Interfaces* **10** 35289–95
[9] Pumera M, Sofer Z and Ambrosi A 2014 *J. Mater. Chem.* A **2** 8981–7
[10] Kvashnin A G, Avramov P V, Kvashnin D G, Chernozatonskii L A and Sorokin P B 2017 *J. Phys. Chem.* C **121** 28484–9
[11] Antipina L Y and Sorokin P B 2015 *J. Phys. Chem.* C **119** 2828–36
[12] Sivek J, Leenaerts O, Partoens B and Peeters F M 2012 *J. Phys. Chem.* C **116** 19240–5
[13] Gao Y, Cao T, Cellini F, Berger C, De Heer W A, Tosatti E, Riedo E and Bongiorno A 2018 *Nat. Nanotechnol.* **13** 133–8
[14] Chernozatonskii L A, Sorokin P B, Kvashnin A G and Kvashnin D G 2009 *JETP Lett.* **90** 134–8
[15] Horbatenko Y, Yousaf M, Lee J, Choi T H, Ruoff R S and Park N 2016 *Carbon* **106** 158–63
[16] Kvashnin A G, Chernozatonskii L A, Yakobson B I and Sorokin P B 2014 *Nano Lett.* **14** 676–81
[17] Odkhuu D, Shin D, Ruoff R S and Park N 2013 *Sci. Rep.* **3** 3276
[18] Hu C H, Zhang P, Liu H Y, Wu S Q, Yang Y and Zhu Z Z 2013 *J. Phys. Chem.* C **117** 3572–9
[19] Li J, Li H, Wang Z and Zou G 2013 *Appl. Phys. Lett.* **102** 073114
[20] Li H, Li J, Wang Z and Zou G 2012 *Chem. Phys. Lett.* **550** 130–3
[21] Zhu L, Hu H, Chen Q, Wang S, Wang J and Ding F 2011 *Nanotechnology* **22** 185202
[22] Zhang Y Y, Wang C M, Cheng Y and Xiang Y 2011 *Carbon* **49** 4511–7
[23] Leenaerts O, Partoens B and Peeters F M 2009 *Phys. Rev.* B **80** 245422
[24] Paul S and Momeni K 2019 *J. Phys. Chem.* C **123** 15751–60
[25] Martins L G P *et al* 2017 *Nat. Commun.* **8** 96
[26] Rajasekaran S, Abild-Pedersen F, Ogasawara H, Nilsson A and Kaya S 2013 *Phys. Rev. Lett.* **111** 085503
[27] Barboza A P M *et al* 2011 *Adv. Mater.* **23** 3014–7
[28] Xie H, Yin F, Yu T, Wang J T and Liang C 2014 *Sci. Rep.* **4** 5930
[29] Xu C *et al* 2013 *Int. J. Refract. Met. Hard Mater.* **36** 232–7
[30] Irifune T, Kurio A, Sakamoto S, Inoue T and Sumiya H 2003 *Nature* **421** 599–600
[31] Wang L, Sofer Z, Šimek P, Tomandl I and Pumera M 2013 *J. Phys. Chem.* C **117** 23251–7
[32] Das D, Hardikar R P, Han S S, Lee K R and Singh A K 2017 *Phys. Chem. Chem. Phys.* **19** 24230–9
[33] Wang X, Zeng Z, Ahn H and Wang G 2009 *Appl. Phys. Lett.* **95** 183103
[34] Sheng Z H, Gao H L, Bao W J, Wang F B and Xia X H 2012 *J. Mater. Chem.* **22** 390–5
[35] Ekimov E A, Sidorov V A, Bauer E D, Mel'nik N N, Curro N J, Thompson J D and Stishov S M 2004 *Nature* **428** 542–5
[36] Bustarret E, Kačmarčik J, Marcenat C, Gheeraert E, Cytermann C, Marcus J and Klein T 2004 *Phys. Rev. Lett.* **93** 237005
[37] Bakharev P V *et al* 2019 (arXiv:1901.02131)
[38] Kresse G and Furthmüller J 1996 *Phys. Rev.* B **54** 11169–86
[39] Kresse G and Furthmüller J 1996 *Comput. Mater. Sci.* **6** 15–50
[40] Kohn W and Sham L J 1965 *Phys. Rev.* **140** A1133–8
[41] Perdew J P, Burke K and Ernzerhof M 1996 *Phys. Rev. Lett.* **77** 3865–8
[42] Pack J D and Monkhorst H J 1977 *Phys. Rev.* B **16** 1748–9
[43] Klimeš J, Bowler D R and Michaelides A 2011 *Phys. Rev.* B **83** 195131
[44] Jiří K, David R B and Angelos M 2010 *J. Phys.: Condens. Matter* **22** 022201
[45] Baroni S, De Gironcoli S, Dal Corso A and Giannozzi P 2001 *Rev. Mod. Phys.* **73** 515–62
[46] Giannozzi P *et al* 2009 *J. Phys.: Condens. Matter* **21** 395502
[47] Bardeen J, Cooper L N and Schrieffer J R 1957 *Phys. Rev.* **108** 1175–204
[48] Panchakarla L S, Subrahmanyam K S, Saha S K, Govindaraj A, Krishnamurthy H R, Waghmare U V and Rao C N R 2009 *Adv. Mater.* **27** 4726–30
[49] Bourgeois E, Bustarret E, Achatz P, Omnès F and Blase X 2006 *Phys. Rev.* B **74** 094509
[50] Takano Y, Nagao M, Sakaguchi I, Tachiki M, Hatano T, Kobayashi K, Umezawa H and Kawarada H 2004 *Appl. Phys. Lett.* **85** 2851–3
[51] Savini G, Ferrari A C and Giustino F 2010 *Phys. Rev. Lett.* **105** 037002
[52] Cheng Y, Wang X, Zhang J, Yang K, Niu C and Zeng Z 2019 *RSC Adv.* **9** 7680–6